PMVictoriaESPPEm Resource

From:	Govan, Tekia
Sent:	Monday, May 16, 2011 12:11 PM
To:	VictoriaESP Resource
Subject:	FW: Exelon Response to NRC RAI Letter No. 07
Attachments:	NP-11-0016 - Response to Request for Additional Information Letter No. 07.pdf

Tekia V. Govan, Project Manager
U.S. Nuclear Regulatory Commission
Office of New Reactors
MS T-6-D48
Washington DC 20555-0001
301-415-6197
Tekia.Govan@nrc.gov

From: Govan, Tekia
Sent: Friday, May 06, 2011 5:07 PM
To: Jones, Henry; Li, Yong; Devlin, Stephanie; Graizer, Vladimir; Gran, Zachary; Williams, Stephen
Subject: FW: Exelon Response to NRC RAI Letter No. 07

All:

Attached is the Exelon Response to NRC RAI Letter No. 07, NP-11-0016, dated May 6, 2011 for section 2.4.6, 2.5.2, and 11.2. EPM will be updated to reflect the MI number once it has been processed through ADAMS.

Tekia
Tekia V. Govan, Project Manager
U.S. Nuclear Regulatory Commission
Office of New Reactors
MS T-6-D48
Washington DC 20555-0001
301-415-6197
Tekia.Govan@nrc.gov

David J. Distel
Exelon Generation
New Plant Regulatory Engineer
Nuclear Project Development
610-765-5517
david.distel@exeloncorp.com

please notify the sender immediately and permanently delete the original and any copy of this e-mail and any printout. Thank You. ***

Hearing Identifier: Victoria_ESP_Public
Email Number: 216

Mail Envelope Properties (F5A4366DF596BF458646C9D433EA37D780CCD5FDFB)

Subject: FW: Exelon Response to NRC RAI Letter No. 07
Sent Date: 5/16/2011 12:10:59 PM
Received Date: 5/16/2011 12:11:01 PM
From: Govan, Tekia

Created By: Tekia.Govan@nrc.gov

Recipients:
"VictoriaESP Resource" <VictoriaESP.Resource@nrc.gov>
Tracking Status: None

Post Office: HQCLSTR01.nrc.gov

Files	Size	Date & Time
MESSAGE	1921	5/16/2011 12:11:01 PM
NP-11-0016 - Response to Request for Additional Information Letter No. 07.pdf	2951903	

Options
Priority: Standard
Return Notification: No
Reply Requested: No
Sensitivity: Normal
Expiration Date:
Recipients Received:

NP-11-0016
May 5, 2011

10 CFR 52, Subpart A

U. S. Nuclear Regulatory Commission
ATTN: Document Control Desk
Washington, DC 20555-0001

Subject: Exelon Nuclear Texas Holdings, LLC
             Victoria County Station Early Site Permit Application
             Response to Request for Additional Information Letter No. 07
             NRC Docket No. 52-042

Attached are responses to NRC staff questions included in Request for Additional Information
(RAI) Letter No. 07, dated April 8, 2011, related to Early Site Permit Application (ESPA), Part 2,
Sections 02.04.06, 02.05.02, and 11.02. NRC RAI Letter No. 07 contained twenty Questions.
This submittal comprises a partial response to RAI Letter No. 07, and includes responses to the
following seven Questions:

02.04.06-1	02.05.02-1	11.02-3
	02.05.02-2	11.02-4
	02.05.02-7	
	02.05.02-8	

When a change to the ESPA is indicated by a Question response, the change will be
incorporated into the next routine revision of the ESPA, planned for no later than
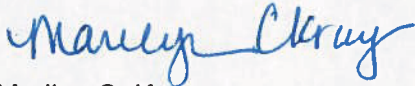March 31, 2012.

The response to RAI Questions 02.04.06-2, 02.05.02-3d, 02.05.02-4, 02.05.02-5, 02.05.02-6a,
02.05.02-6b, and 02.05.02-9 will be provided by May 23, 2011. The response RAI Question
02.05.02-6c will be provided by June 22, 2011. The response to RAI Questions 02.04.06-3 and
02.05.02-10 will be provided by July 7, 2011. The response to RAI Questions 02.05.02-3a,
02.05.02-3b, and 02.05.02-3c will be provided by August 5, 2011. These response times are
consistent with the response times described in NRC RAI Letter No. 07, dated April 8, 2011.

Regulatory commitments established in this submittal are identified in Attachment 8. If any
additional information is needed, please contact David J. Distel at (610) 765-5517.

I declare under penalty of perjury that the foregoing is true and correct. Executed on the 5th day of May, 2011.

Respectfully,

Marilyn C. Kray
Vice President, Nuclear Project Development

Attachments:
1. Question 02.04.06-1
2. Question 02.05.02-1
3. Question 02.05.02-2
4. Question 02.05.02-7
5. Question 02.05.02-8
6. Question 11.02-3
7. Question 11.02-4
8. Summary of Regulatory Commitments

cc: USNRC, Director, Office of New Reactors/NRLPO (w/Attachments)
        USNRC, Project Manager, VCS, Division of New Reactor Licensing (w/Attachments)
        USNRC, Environmental Project Manager, VCS, Division of New Reactor Licensing
            (w/Attachments)
        USNRC Region IV, Regional Administrator (w/Attachments)

RAI 02.04.06-1:

Question:

To meet the requirements of GDC 2, 10 CFR 52.17, and 10 CFR Part 100, an assessment of the Probable Maximum Tsunami (PMT) for the proposed site should be provided in the application. Section C.I.2.4.6.3 of Regulatory Guide 1.206 (RG 1.206) provides specific guidance with respect to the source characteristics needed to determine the PMT. These characteristics include detailed geo-seismic descriptions of the controlling local tsunami generators, including location, source dimensions, and maximum displacement. Provide additional information, evaluation and a discussion in the SSAR of the following:

(1) Why major Gulf of Mexico and Caribbean landslides other than the East Breaks slump were excluded as potential tsunamigenic sources for the PMT, particularly those landslides along the Mississippi Canyon, west Florida Slope/Escarpment, and Campeche Escarpment.

(2) The differences in maximum earthquake magnitudes used in Section 2.4.6.1 and in Section 2.5.2 and why the lower maximum magnitudes are used in regard to tsunami source parameters. Also, provide discussion of the source parameters of recent earthquakes that have occurred in the Gulf of Mexico in regard to tsunami generation.

(3) Clarification and justification of the dissipation statement that assume the amplitude of any tsunami wave from outside the Gulf of Mexico (specifically Caribbean sources) would be reduced by traveling through the Florida Straits or would be blocked by the Bahamas.

(4) The location and the tsunamigenic potential of volcanoes near the coast of the Gulf of Mexico in relation to their potential as a PMT source.

(5) Clarification on how the mid-Holocene age of the Mississippi Canyon landslide relates to establishing this region as potentially active, especially in terms of the whether the age is used to exclude the landslide from consideration as a potential PMT source and if so, why.

(6) Updated information, using recently published sources or independent evaluation, on the tsunami source parameters used for the East Breaks slump.

Response:

Response Item (1):

Responses to Item (1) are provided in two parts. Part (a) addresses potential tsunami generation from submarine landslides in the Gulf of Mexico. Part (b) addresses potential tsunami generation from submarine landslides in the Caribbean region.

Part (a): Potential Tsunami Generation from Submarine Landslides in the Gulf of Mexico.

SSAR Subsection 2.4.6.3 states that "it is postulated that the tsunami source that could produce a PMT at the Texas Gulf Coast would be a submarine landslide within the Gulf of Mexico." With respect to the PMT source, SSAR Subsection 2.4.6.1 states that "the major tsunami sources from near-field landslides reside within the Gulf of Mexico. The Gulf of Mexico is characterized by three geologic provinces: the Carbonate, Salt, and Canyon/Fan as shown in Figure 2.4.6-1." SSAR Figure 2.4.6-1 also shows potential source areas within each province, including the East

Breaks slump, the west Florida Slope/Escarpment, the Campeche Escarpment, and the Mississippi Canyon.

The postulated SMF sources in the carbonate province are located offshore of West Florida and in the Campeche Escarpments north of the Yucatan Peninsula. The largest SMF scar in this region is along the central part of the West Florida Slope and is estimated as 120 km long, 30 km wide, with a total volume of material removed of about 1,000 km^3. However, the formation of the scar was believed to have occurred as a result of multiple events. Most of the sediment was believed to have been removed before the middle of the Miocene.

The salt province is located in the northwestern Gulf of Mexico. As stated in SSAR Subsection 2.4.6.3, thirty-seven landslides were identified in the salt province and along the base of the Sigsbee Escarpment. The largest documented SMF scar in the salt province is the East Breaks slump (Reference 1).

Lastly, three canyon/fan systems are present in the canyon to deep-sea fan province: the Bryant, the Mississippi, and the Eastern Mississippi systems (Reference 1). These fan systems were formed during the Pliocene and Pleistocene. The Mississippi Fan is the largest of the three fans. The largest landslide in the complex covers approximately 23,000 km^2 and reaches 100 m in thickness, with a volume estimated to be on the order of 1,725 km^3. However, Geologic Long-Range Inclined Asdic (GLORIA) imagery suggests that this feature consists of at least two separate events (Reference 1). The resumption of hemipelagic sedimentation in the head of the Mississippi Canyon by 7500 years before the present indicates that the largest of the landslide complexes ceased being active by the middle of the Holocene, which is discussed further in the response to Item (5) below.

The East Breaks slump was selected as the PMT based on the source parameters that are described in Item (6) of this response and the proximity to the VCS site. For example, the VCS site is located about 36 mi (58 km) from the South Texas coast and about 105 mi (169 km) from the East Breaks slump (SSAR Figure 2.4.6-1). The VCS site is located about 430 mi (692 km), 520 mi (837 km), and 750 mi (1207 km), respectively, from the Mississippi Canyon, Campeche Escarpment, and west Florida Slope/Escarpment, respectively. As compared with potential source parameters for the East Breaks slump, SMF sources located in remote areas of the Gulf of Mexico are not expected to represent the limiting source mechanism for the PMT for the VCS site.

Part (b): Potential Tsunami Generation from Submarine Landslides in the Caribbean Region.

With respect to far-field landslides in the Caribbean region, this source was not considered as a potential tsunamigenic source for the PMT for reasons as described below.

- There are few studies that characterize potential landslide-induced tsunami sources within the Caribbean region. Among them, McCann (Reference 4) developed a map of "reference tsunami amplitudes" for the Caribbean region based on depth and slopes of sea floors and hypothetical submarine slides of 20 meter thick and 1 km long. In the study, McCann concludes that landslides are most tsunamigenic in shallower waters, and therefore, steeper regions near island platforms are typically regions of high tsunami potential. However, tsunamis generated by landslides have impact at the near-field coastal areas more than at far-field locations (References 2 and 3). As indicated by Pararas-Carayannis (Reference 3), the heights of tsunami waves generated from landslides within the Caribbean region attenuate rapidly with distance, because of relatively smaller source dimensions and shorter wave periods, and thus do not pose a significant danger at great distances from the source. In contrast, earthquake-generated

tsunamis have relatively high levels of energy, can travel for a very long distance over open sea, and can result in substantial coastal flooding.

- Because of the regional and local effects of landslide-induced tsunamis, Reference 2 states that potential tsunami sources for the Gulf of Mexico are submarine landslides within the Gulf of Mexico.

- The study by Knight (SSAR Reference 2.4.6-2) performed model simulations for hypothetical tsunami sources placed in the Atlantic, the Gulf of Mexico and in the Caribbean, and concluded that "sources outside the Gulf are not expected to create a tsunami threatening to the Gulf coast." The conclusion is attributed to the reasoning that "the Atlantic and Gulf coasts are nearly independent since the hydrodynamic connection between basins is through the narrow Straits of Florida and through the Caribbean, where bottom friction losses appear to be large." (SSAR Reference 2.4.6-2).

Therefore, tsunamis generated due to landslides in the Caribbean region are not expected to pose a flooding risk to the safety-related functions of VCS.

Response Item (2)

The response to Item (2) was provided as a response to Hydrology Information Need (INH) 19, submitted to the NRC under Exelon Letter No. NP-11-0007, dated February 10, 2011.

Response Item (3)

Tsunami propagation simulations from hypothetical large-magnitude earthquakes located outside the Gulf of Mexico were performed in the study by Knight (2006) (SSAR Reference 2.4.6-2) and for Reference 1. Potential tsunami propagation into the Gulf of Mexico from large-magnitude earthquakes was also discussed in Reference 5. As stated in SSAR Reference 2.4.6-2, "propagation into the Gulf [of Mexico] takes two routes, one through the Caribbean and the other through the Straits of Florida." Reference 2.4.6-2 stated that the "Atlantic and Gulf coasts are nearly independent since the hydrodynamic connection between basins is through the narrow Straits of Florida and through the Caribbean, where bottom friction losses appear to be large."

SSAR Reference 2.4.6-2 provides information on the level of tsunami threat between basins and concludes that "sources outside the Gulf are not expected to create a tsunami threatening to the Gulf coast." Similarly, Reference 5 states that "tsunami propagation from significant earthquake sources outside the Gulf of Mexico, such as the northern Panama Convergence Zone, Northern South America, Cayman Trough, the Puerto Rico trench, or the Gibraltar area shows that wave amplitude is greatly attenuated by the narrow and shallow passages into the gulf, and as a result, these tsunami sources do not constitute a tsunami hazard to the Gulf of Mexico coast."

For tsunami propagation through the Caribbean, Reference 1 states that:

> "in general, these [tsunami propagation simulation] results are consistent with the findings of Knight (2006) [Reference 2.4.6-2], where the far-field tsunamis generated from earthquakes located beneath the Caribbean Sea are higher along the Gulf coast than the Atlantic coast because of dissipation through the Greater Antilles islands. Conversely, tsunamis generated from earthquakes north of the Greater Antilles are higher along the Atlantic coast than the Gulf coast."

For tsunami propagation through the Florida Straits, Reference 1 states that the Bahamas may act as a barrier. For example, for the 1755 tsunami that occurred as the result of a large earthquake near Lisbon, Portugal, Reference 1 states that "we believe the reason why there are no reports from the 1755 tsunami in southern Florida could be attributed to the northern Bahamas Banks (NBB) which may have acted as a barrier to that area."

Therefore, tsunamis generated due to large-magnitude earthquakes outside of the Gulf of Mexico are not expected to pose a flooding risk to the safety-related functions of VCS.

Response Item (4)

The National Geophysical Data Center (NGDC) natural hazard database for volcanoes (Reference 6) lists only two volcanoes near the Gulf Coast (Los Atlixcos and San Martin). Both volcanoes are located near Veracruz, Mexico. Los Atlixcos is located about 9 km (5.6 mi) from the Gulf Coast and about 975 km (606 mi) from the VCS site. San Martin is located about 13 km (8.0 mi) from the Gulf Coast and about 1127 km (700 mi) from the VCS site. Reference 5, which provided a regional assessment of tsunami potential in the Gulf of Mexico, did not discuss any volcanoes near the Gulf of Mexico as potential tsunamigenic sources. Also, Reference 1 stated that volcanogenic sources are unlikely to be the causative tsunami generator for damaging tsunamis in the Gulf of Mexico region. Therefore, volcanogenic sources are not considered as a limiting source mechanism for the PMT or as a flooding hazard to the safety-related functions of VCS.

Response Item (5)

With respect to landslides in the Mississippi Canyon as a potential PMT source, USGS (2008) (Reference 1) states that "borings and seismic data from the head of Mississippi Canyon indicate that there were alternating episodes of canyon filling and excavation between 19,000 and 7,500 years before the present." In addition, as stated in the response to Item (1), GLORIA imagery of the Mississippi Fan suggests that this feature consists of at least two separate events (Reference 1). Reference 1 also states that "the resumption of hemipelagic sedimentation in the head of Mississippi Canyon by 7,500 years before the present indicates that at least the largest of these landslide complexes had ceased being active by mid-Holocene time." Therefore, large landslides in the Mississippi Canyon are not considered as an active source mechanism for the PMT and are not considered further.

Response Item (6)

Estimates of dimensions of the East Breaks slump scar have varied with different investigations. For example, source parameters for the East Breaks slump scar are provided in Reference 1. Source parameters for the East Breaks slump were also estimated independently from three-arc-second bathymetry data from the National Geophysical Data Center (NGDC) (Reference 7). Slump width was estimated to be approximately 13.4 km (Figure 1). The length of the erosional chute was estimated to be about 42 km. Based on a transect across the erosional chute, slump thickness was estimated to be about 100 m (i.e., see cross-section profile A to A' in Figure 1). With respect to slope, SSAR Reference 2.4.6-3 stated that "initial failure of the slump took place on very low angle slopes of less than two degrees while present slump deposits have an average seafloor slope of one-degree." While a vertical drop of 850 m over a length of 42 km indicates a bed slope of approximately 1.1 degrees, a maximum local slope of 2 degrees was used as a conservative estimate. Similarly, initial depth of the slide was estimated conservatively at the depth of the midpoint between the 200-m and 1000-m bathymetry contour elevations. Therefore, initial depth was estimated to be 600 m (i.e., (200 m + 1000 m)/2). Reference 1, citing interpretation of side-scan sonar data by Reference 8, estimated the length of the East Breaks slump as 114 km. Therefore, the total slide length was assumed to be 114 km.

References:

1. Atlantic and Gulf of Mexico Tsunami Hazard Assessment Group, *Evaluation of tsunami sources with the potential to impact the U.S. Atlantic and Gulf coasts – An updated report to the Nuclear Regulatory Commission*: U.S. Geological Survey Administrative Report, August 2008.

2. Kammerer, A., ten Brink, U., and Titov, V., *Overview of the U.S. Nuclear Regulatory Commission collaborative research program to assess tsunami hazard for nuclear power plants on the Atlantic and Gulf coasts*, The 14th World Conference on Earthquake Engineering, October 12–17, 2008, Beijing, China.

3. Pararas-Carayannis, G., *Volcanic tsunami generating source mechanisms in the eastern Caribbean region*, Science of Tsunami Hazards, 22(2): 74–114, 2004.

4. McCann, W., *Estimating the threat of tsunamigenic earthquakes and earthquake induced-landslide tsunami in the Caribbean*, Caribbean Tsunami Hazards, Proceedings of the NSF Caribbean Tsunami Workshop, Mercado-Irizarry, A. and Liu, P. (eds.), 43–65, World Scientific Publishing Co. Pte. Ltd., Singapore, 2006.

5. ten Brink, U., Twichell, D., Lynett, P., Geist, E., Chaytor, J., Lee, H., Buczkowski, B. and C. Flores, 2009, *Regional Assessment of Tsunami Potential in the Gulf of Mexico: U.S. Geological Survey Administrative Report*, Report to the National Tsunami Hazard Mitigation Program, United States Geological Survey, Date: September 2, 2009.

6. National Geophysical Data Center (NGDC), 2010, *Volcano Location Database Search*, National Oceanic and Atmospheric Administration (NOAA), available at http://www.ngdc.noaa.gov/nndc/struts/form?t=102557&s=5&d=5, accessed May 2, 2011.

7. National Geophysical Data Center (NGDC), 2008, *GEODAS Grid Translator*, National Oceanic and Atmospheric Administration (NOAA), available at http://www.ngdc.noaa.gov/mgg/gdas/gd_designagrid.html, accessed July 26, 2008.

8. Rothwell, R.G., Kenyon, N.H. and B.A. McGregor, *Sedimentary Features of the South Texas Continental Slope as Revealed by Side-Scan Sonar and High-Resolution Seismic Data*, The American Association of Petroleum Geologists Bulletin 75(2): 298-312, 1991.
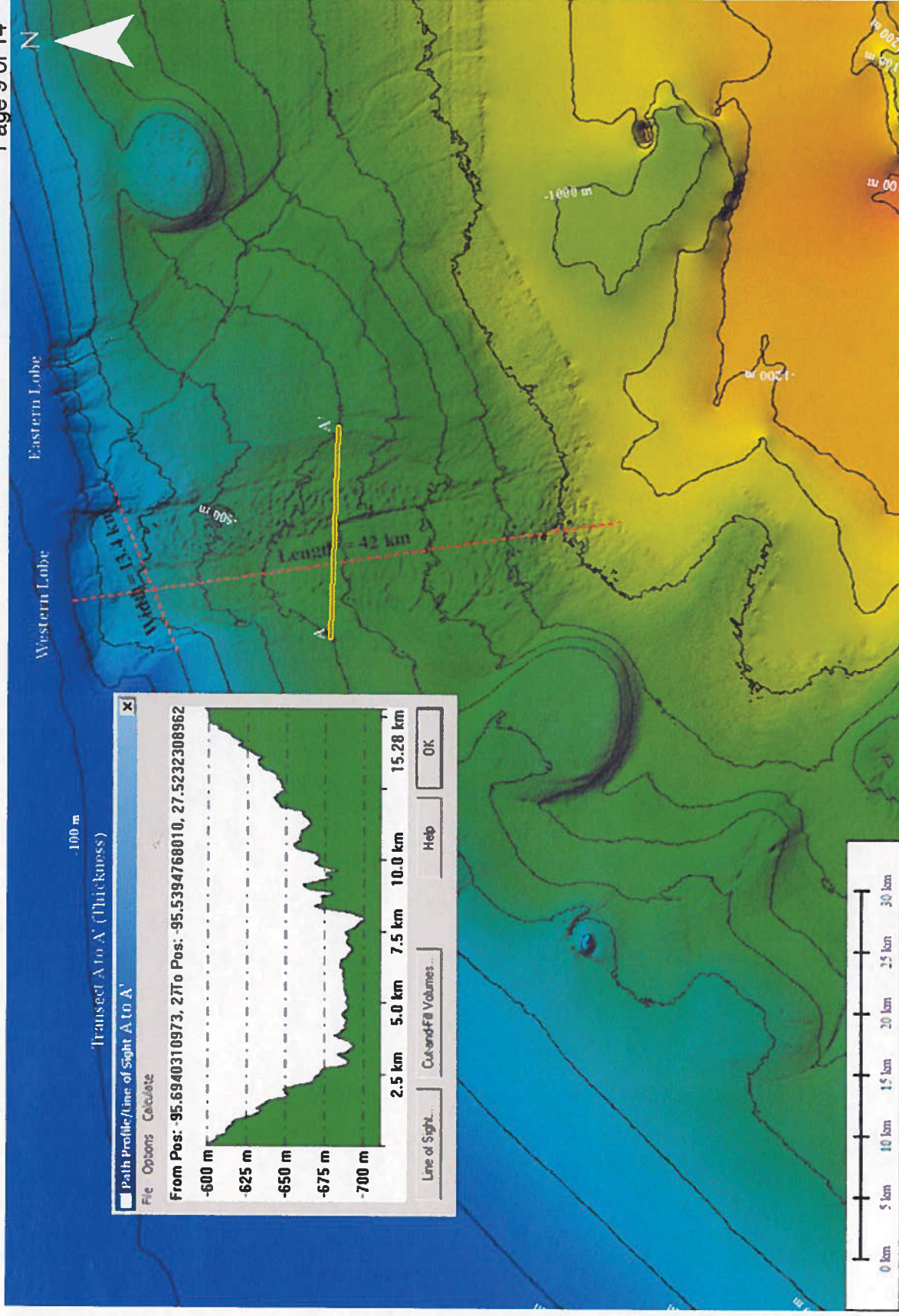
Figure 1. Dimensions of East Breaks slump scar. Source of data: NGDC (2008) (Reference 6).

Associated ESPA Revisions:

In response to this RAI, the second paragraph of SSAR Subsection 2.4.6.1, Revision 0 will be revised as follows:

The major tsunami sources from far-field landslides include submarine landslide zones along the U.S. Atlantic Margin, the Nova Scotia Margin ~~in~~on the eastern Canada coast northeast of the U.S. border, the Caribbean region, the Storegga landslide zone in the northern Atlantic Ocean east of Iceland, and the Puerto Rico Trench (Reference 2.4.6-1). Based on the locations and mechanisms of these sources provided in Reference 2.4.6-1, submarine landslides along the U.S. Atlantic Margin, from the eastern end of the Georges Bank, New England, to the Blake Spur near the Carolina Trough, would generate the most significant tsunami that may affect the Texas Gulf Coast. Numerical model simulations of tsunami propagation show that the tsunami impact along the Atlantic Coast would be considerably reduced due to the presence of a wide continental shelf (Reference 2.4.6-1). There is currently no literature on tsunami model simulation within the Gulf of Mexico from the U.S. Atlantic Margin sources. ~~However, because tsunami waves from these sources would be dissipated by traveling over the shallow shelf of the Florida Strait to reach the Gulf of Mexico, the tsunami amplitude at the Texas Gulf Coast would be further reduced. A similar behavior of tsunami propagation and dissipation has been reported in computer model simulations of the Puerto Rico Trench earthquake-generated tsunamis (Reference 2.4.6-2).~~ However, the study by Knight (Reference 2.4.6-2) performed model simulations for hypothetical tsunami sources placed in the Atlantic, the Gulf of Mexico and in the Caribbean, and concluded that "sources outside the Gulf are not expected to create a tsunami threatening to the Gulf coast." The conclusion is attributed to the reasoning that "the Atlantic and Gulf coasts are nearly independent since the hydrodynamic connection between basins is through the narrow Straits of Florida and through the Caribbean, where bottom friction losses appear to be large." (Reference 2.4.6-2).

In response to this RAI, SSAR Subsection 2.4.6.1, Revision 0 will be revised by adding the following paragraph between the second and the third paragraphs:

Potential far-field submarine landslide tsunami sources in the Caribbean Basin are those areas along relatively steep slopes adjacent to islands and to seismic sources (Reference 2.4.6-13). As indicated in Reference 2.4.6-13, submarine landslides are most tsunamigenic in shallower waters, and, therefore, steeper regions near island platforms are typically regions of high tsunami potential. Most of the landslides are activated by seismic activity. As indicated above, tsunamis generated in the Atlantic/Caribbean are not expected to affect the Gulf of Mexico because of large friction losses in the Caribbean basin and relatively narrow connections between the basins. In addition, tsunamis generated by landslides impact near-field coastal areas more than far-field locations (References 2.4.6-14 and 2.4.6-15). As discussed in Reference 2.4.6-15, the heights of tsunami waves generated from landslides attenuate rapidly with distance because of relatively smaller source dimensions and shorter wave periods and do not pose a significant danger at great distances from the source. Therefore, far-field, landslide-generated tsunamis in the Caribbean region are not expected to pose a flooding hazard in the Gulf of Mexico.

In response to this RAI, the ninth paragraph of SSAR Subsection 2.4.6.1, Revision 0 will be revised as follows:

While volcanism and volcanism-based tsunamis have been reported in the Caribbean and Canary Islands (Reference 2.4.6-7), no such tsunamis have been documented in the Gulf of Mexico. The last postulated tsunami in the Atlantic Ocean may have been associated with the

eruption and lateral flank failure of the Cumbre Vieja, a volcano on the Island of La Palma in the Canary Islands, about 550,000 years ago (Reference 2.4.6-7). It is, however, not expected to cause a destructive tsunami along the east or Gulf Coast of the U.S as indicated by numerical simulation results (Reference 2.4.6-1). As Reference 2.4.6.-17 stated that volcanogenic sources are unlikely to be the causative tsunami generator for damaging tsunamis in the Gulf of Mexico region, and volcanoes located near the Gulf of Mexico (Reference 2.4.6-19) are not discussed as a potential tsunamigenic mechanism in Reference 2.4.6-18, volcanogenic sources are not considered as a limiting source mechanism for the PMT or as a flooding hazard to the safety-related functions of VCS.

In response to this NRC request, the first paragraph of SSAR Subsection 2.4.6.3, Revision 0 will be revised as follows:

From the discussion presented above, it is postulated that the tsunami source that could produce a PMT at the Texas Gulf Coast would be a submarine landslide within the Gulf of Mexico. There is no record of tsunamis from this source. Reference 2.4.6-17 cites four credible submarine mass failure (SMF) source areas in the Gulf of Mexico: the Florida Escarpment, Campeche Escarpment, the Mississippi Canyon, and the Northwest Gulf of Mexico (Figure 2.4.6-1). These four SMF source areas are located in three geologic provinces: a carbonate province, a canyon to deep-sea fan province, and a salt province.

The postulated SMF sources in the carbonate province are located offshore of West Florida and in the Campeche Escarpments north of the Yucatan Peninsula (Reference 2.4.6-17). The largest scar in this region is along the central part of the West Florida Slope and is estimated as 120 km long, 30 km wide, with a total volume of material removed of about 1,000 km^3. However, formation of the scar was believed to have occurred as a result of multiple events. Most of the sediment was estimated to have been removed before the middle of the Miocene. Reference 2.4S.6-17 stated the following:

> "During the Mesozoic, an extensive reef system developed around much of the margin of the Gulf of Mexico Basin by the vertical growth of reefs and carbonate shelf edge banks. This reef system is exposed along the Florida Escarpment and the Campeche Escarpment that fringe the eastern and southern margins of this basin. These escarpments stand as much as 1,500 m above the abyssal plain floor, and have average gradients that commonly exceed 20° and locally are vertical. Reef growth ended during the Middle Cretaceous, and subsequently the platform edges have been sculpted and steepened by a variety of erosional processes."

~~The earthquake tsunami sources in the Caribbean Basin frequently generated tsunamis in that region. However, for the Texas Gulf Coast shoreline, the postulated tsunami event due to the hypothetical landslide within the Gulf Basin would be considerably more severe than the earthquake-generated tsunamis.~~

In response to this NRC request, the second paragraph of SSAR Subsection 2.4.6.3, Revision 0 will be revised as follows:

The largest landslide complex that was mapped by the USGS in the Gulf Basin is in the middle and upper Mississippi Canyon/Fan province (Reference 2.4.6-1). The area of the landslide complex is estimated to be approximately 23,000 square kilometers (8880 square miles), with a maximum thickness of about 100 meters (328 feet), and a total volume of approximately 1725 cubic kilometers (414 cubic miles). However, the characteristic dimensions of the slide that may

be used to generate a tsunami in the Gulf of Mexico are not available (Reference 2.4.6-1). Borings and seismic data from the head of Mississippi Canyon indicate that there were alternating episodes of canyon filling and excavation between 19,000 and 7,500 years before the present (YBP). Also, Geologic Long-Range Inclined Asdic (GLORIA) imagery of the Mississippi Fan suggests that this feature consists of at least two separate events (Reference 2.4.6-17). ~~The landslide complex is indicated to have ceased being active by mid-Holocene time.~~. The resumption of hemipelagic sedimentation in the head of Mississippi Canyon by 7,500 YBP indicates that at least the largest of these landslide complexes had ceased being active by mid-Holocene time.

In response to this RAI, the fourth paragraph of SSAR Subsection 2.4.6.3, Revision 0 will be revised as follows:

Estimates of dimensions of the East Breaks slump scar have varied with different investigations. Reference 2.4.6-1 characterizes the East Breaks slump to have a 20 kilometer (12.5 miles) wide head scarp at about the 180 meters (590 feet) isobath, and a slide complex area of approximately 3200 square kilometers (1236 square miles). The estimated length of the slide (erosional) is about 55 kilometers (34 miles), and the maximum thickness of the slump is about 70 meters (230 feet). The total estimated volume of the slide is about 50 to 60 cubic kilometers (12 to 14 cubic miles). Source parameters for the East Breaks slump were also estimated independently from three-arc-second bathymetry data from the National Geophysical Data Center (NGDC) (Reference 2.4.6-16). Slump width was estimated to be approximately 13.4 km (Figure 2.4.6-7). The length of the erosional chute was estimated to be about 42 km. Based on a transect across the erosional chute, slump thickness was estimated to be about 100 m (i.e., see cross-section profile A to A' in Figure 2.4.6-7). With respect to slope, Reference 2.4.6-3 stated that "initial failure of the slump took place on very low angle slopes of less than two degrees while present slump deposits have an average seafloor slope of one-degree." While a vertical drop of 850 m over a length of 42 km indicates a bed slope of approximately 1.1 degrees, a maximum local slope of 2 degrees was used as a conservative estimate. Similarly, initial depth of the slide was estimated conservatively at the depth of the midpoint between the 200-m and 1000-m bathymetry contour elevations. Therefore, initial depth was estimated to be 600 m (i.e., (200 m + 1000 m)/2). Reference 2.4.6-17, citing interpretation of side-scan sonar data by Reference 2.4.6-20, estimated the length of the East Breaks slump as 114 km. Therefore, the total slide length was assumed to be 114 km.

In response to this RAI, SSAR Subsection 2.4.6.8, Revision 0 will be revised by adding the following references after Reference 2.4.6-12:

2.4.6-13 McCann, W., *Estimating the threat of tsunamigenic earthquakes and earthquake induced-landslide tsunami in the Caribbean*, Caribbean Tsunami Hazards, Proceedings of the NSF Caribbean Tsunami Workshop, Mercado-Irizarry, A. and Liu, P. (eds.), 43–65, World Scientific Publishing Co. Pte. Ltd., Singapore, 2006.

2.4.6-14 Kammerer, A., ten Brink, U., and Titov, V., *Overview of the U.S. Nuclear Regulatory Commission collaborative research program to assess tsunami hazard for nuclear power plants on the Atlantic and Gulf coasts*, The 14th World Conference on Earthquake Engineering, October 12–17, 2008, Beijing, China.

2.4.6-15 Pararas-Carayannis, G., *Volcanic tsunami generating source mechanisms in the eastern Caribbean region*, Science of Tsunami Hazards, 22(2): 74–114, 2004.

2.4.6-16 National Geophysical Data Center (NGDC), 2008, GEODAS Grid Translator, National Oceanic and Atmospheric Administration (NOAA), available at http://www.ngdc.noaa.gov/mgg/gdas/gd_designagrid.html, accessed July 26, 2008.

2.4.6-17 Atlantic and Gulf of Mexico Tsunami Hazard Assessment Group, 2008, *Evaluation of Tsunami Sources with the Potential to Impact the U.S. Atlantic and Gulf Coasts - A Report to the Nuclear Regulatory Commission*: U.S. Geological Survey Administrative Report, Revision: August 22, 2008.

2.4.6-18 ten Brink, U., Twichell, D., Lynett, P., Geist, E., Chaytor, J., Lee, H., Buczkowski, B. and C. Flores, 2009, Regional Assessment of Tsunami Potential in the Gulf of Mexico: U.S. Geological Survey Administrative Report, Report to the National Tsunami Hazard Mitigation Program, United States Geological Survey, Date: September 2, 2009.

2.4.6-19 National Geophysical Data Center (NGDC), 2010, Volcano Location Database Search, National Oceanic and Atmospheric Administration (NOAA), available at http://www.ngdc.noaa.gov/nndc/struts/form?t=102557&s=5&d=5, accessed May 2, 2011.

2.4.6-20 Rothwell, R.G., Kenyon, N.H. and B.A. McGregor, Sedimentary Features of the South Texas Continental Slope as Revealed by Side-Scan Sonar and High-Resolution Seismic Data, The American Association of Petroleum Geologists Bulletin 75(2): 298-312, 1991.

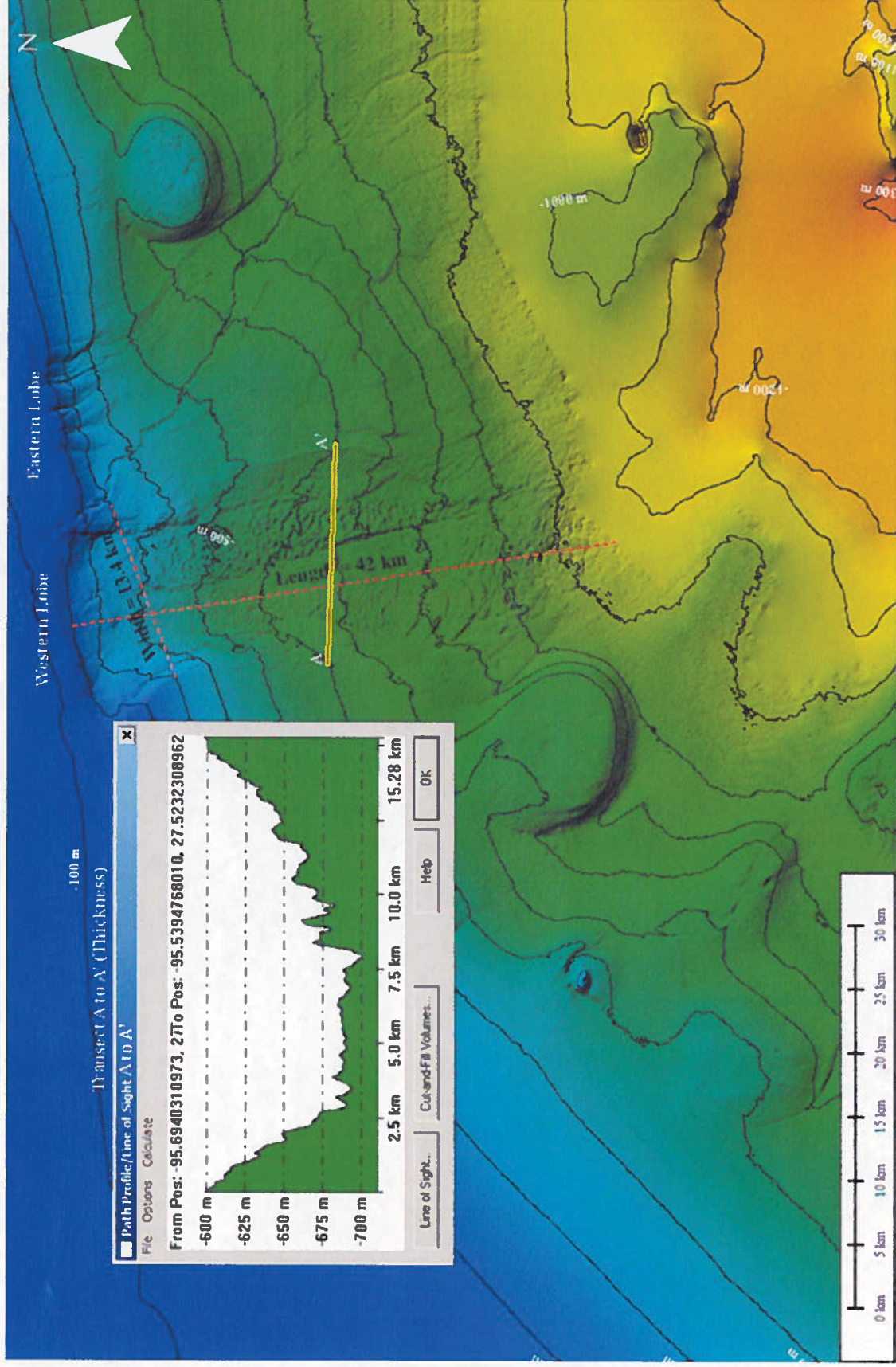In response to this RAI, Figure 2.4.6-7 will be added:

Figure 2.4.6-7 Source parameters for East Breaks slump - Bathymetry elevations are relative to MSL. (Source of bathymetry data: Reference 2.4.6-16)

RAI 02.05.02-1:

Question:

In SSAR Section 2.5.2.1, the applicant discussed its seismicity catalog. In accordance with 10 CFR 100.23, the staff requests the applicant provide additional information regarding its seismicity catalog.

a) The following four earthquakes are reported by the USGS PDE earthquake catalog and occur within 320-km (200-mi) of the VCS site. These four earthquakes do not appear in the applicant's updated seismicity catalog in SSAR Table 2.5.2-3.

```
PDE  1991  0720233819.2  28.91 -98.04  10  3.40LgTUL 3.60LgGS
PDE  1993  0409122919.1  28.81 -98.12  5             4.30LgGS
PDE  1993  0516153019.3  28.81 -98.17  5             3.00LgGS
PDE  1997  0324223134.5  27.72 -98.05  5             3.80LgGS
```

In addition, SSAR Figure 2.5.2-1 appears to show fewer events than a plot of the PDE events within the same investigation window.

Please discuss these apparent discrepancies between the applicant's updated seismicity catalog and USGS PDE catalog and the impact on hazard at the VCS site.

b) In SSAR Section 2.5.2.1.2.1, the applicant stated that "body wave magnitude was related to moment magnitude using the arithmetic average of three equations, or their inversions." Please provide more detail on the magnitude conversion methods and their corresponding inversions.

Response:

Response (a):

Four PDE Events

Exelon considered the four PDE events identified in the RAI during the development of the catalog update. {These events are also listed in other seismicity catalogs considered during the catalog update including ANSS, ISC, and FDNC.} The FDNC seismicity catalog is a catalog of seismic events as referenced to the book, "*Texas Earthquakes*" (Frohlich and Davis, 2002) included as SSAR Reference 2.5.2-4.

During the seismicity catalog development, and in consultation with Dr. Cliff Frohlich, professor of seismology at the University of Texas and co-author of the book referenced above, these four events were identified as *man-made* and removed from the catalog of tectonic events.

More specifically, the first three events are discussed in Davis et al. (Reference 1), where it is "*strongly suggested*" that these events were induced by fluid withdrawal

related to ongoing oil and gas production. In Table 9.3 of SSAR Reference 2.5.2-4, these three events are classified as "probably man-made (induced)".

In SSAR Reference 2.5.2-4 the 1997 event, which is referred to as "Alice—24 March 1997", is also identified as "*man-made*". Figure 9.28 from this reference shows the felt area map contours of this event centered immediately adjacent to an identified major oil field. In Table 9.3 of this reference, the 1997 event is classified as "probably man-made (induced)".

Figure 2.5.2-1 vs. USGS PDE Catalog

Using the PDE (NEIC) catalog obtained to update the seismicity catalog for the SSAR in 2007, and processing the PDE type-specific magnitudes to obtain Emb -- as discussed in the SSAR -- for the same geographic window (83° to 107°W, 24° to 40°N), magnitudes (Emb ≥ 3.0), and primary update period (1985 – 2007), the resulting PDE seismicity is shown in Figure 1, below.}   Figure 1 indicates that there are actually more earthquakes in the SSAR Figure 2.5.2-1 (491 events) than given by the PDE catalog alone (439 events) under the search parameters identified above. (Note that only the explicit Gulf of Mexico area (24°N to 32°N, 100°W to 83°W) was updated for all time, as discussed in the SSAR, and six additional pre-1985 events for the Gulf of Mexico area are tabulated in SSAR Table 2.5.2-2.)

As discussed above, it appears that SSAR Figure 2.5.2-1 shows more earthquakes than given by the PDE (NEIC) catalog alone. It is noted that the PDE catalog was considered in the development of the updated seismicity catalog along with several other catalogs that had events not given in the PDE catalog. Based on processing for priority catalogs in the event of multi-source catalog duplication, as well as removing events assessed to be man-made – including the four PDE events highlighted in this RAI, Exelon concludes there is no discrepancy between the PDE and SSAR seismicity catalogs; therefore, there is no impact on the hazard for the VCS site.
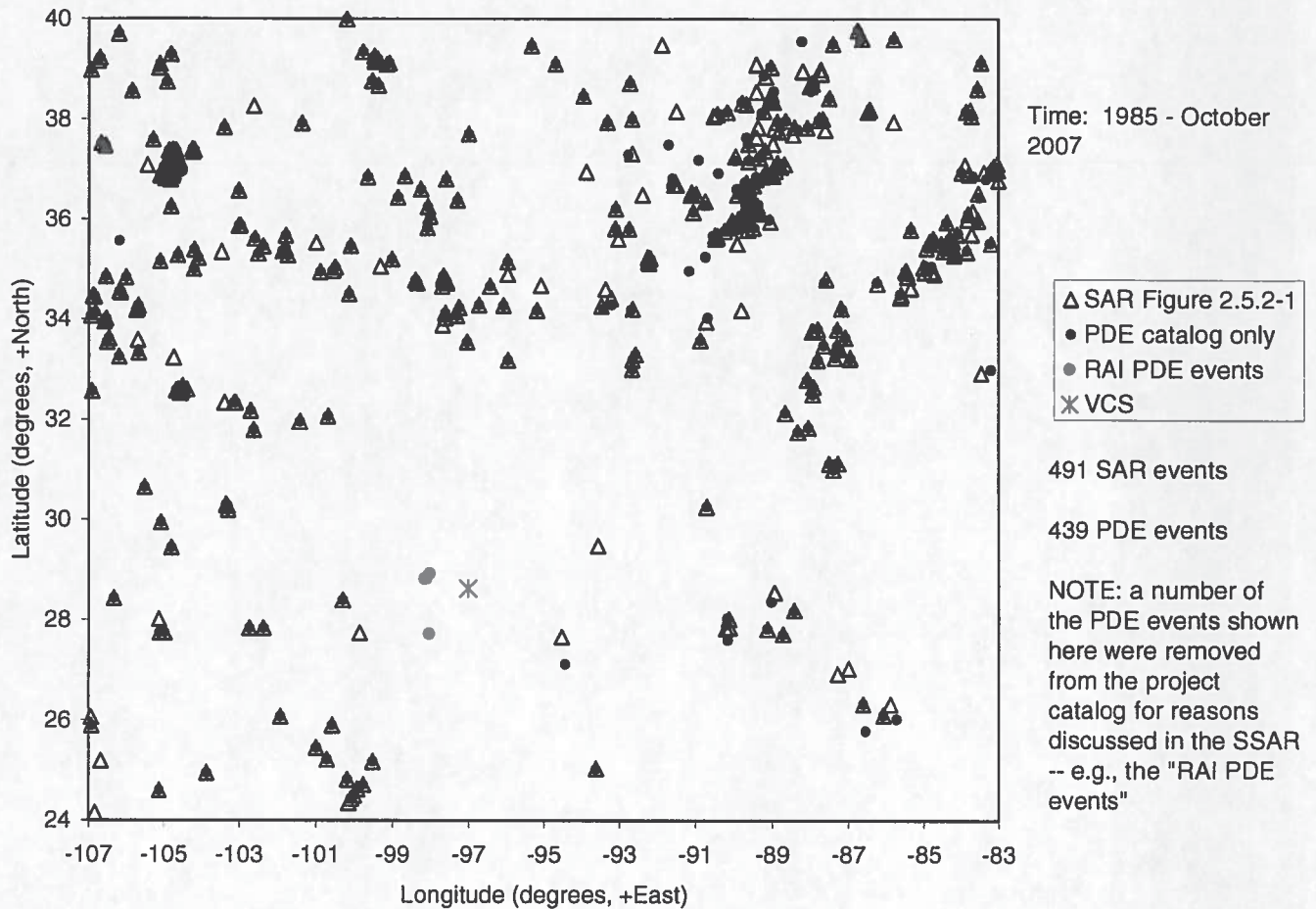
Figure 1. Comparison of the updated seismicity catalog and the PDE catalog

Note: The four red PDE events are the events referred to in the RAI, which have
been identified as man-made.

Response (b):

SSAR Section 2.5.2.1.2.1 states the following:

"The EPRI PSHA study expressed maximum magnitude (M_{max}) values in terms of body-wave magnitude (m_b), whereas most modern seismic hazard analyses describe M_{max} in terms of moment magnitude (M_w). To provide a consistent comparison between magnitude scales, body-wave magnitude was related to moment magnitude using the arithmetic average of three equations, or their inversions, presented by Atkinson and Boore (Reference 2.5.2-13), Frankel et al. (Reference 2.5.2-14), and EPRI (Reference 2.5.2-15). Throughout the description in Subsections 2.5.2.2 and 2.5.2.3, the largest values of M_{max} distributions assigned by the Earth Science Teams (EST) (Reference 2.5.2-16) to seismic sources are presented for both magnitude scales (m_b and M_w). For example, EPRI m_b values of M_{max} are followed by the equivalent M_w value. Conversion values from m_b to M_w and M_w to m_b are provided in Table 2.5.2-1. m_b magnitudes converted from moment magnitudes in this fashion were considered estimates of Emb."

The conversion between M_w to m_b is the same as that considered in EPRI 2004 (see Appendix H to SSAR Reference 2.5.2-98). The explicit formulation of this magnitude conversion is as follows.

If given m_b [m_{bLg}, m_N, m_{Lg}, or m_b] and need M_w, then

$$M_w = (M_{w1} + M_{w2} + M_{w3})/3$$

where

$$M_{w1} = -0.39 + 0.98* m_b \qquad m_b \leq 5.5$$
$$= 2.715 - 0.277* m_b + 0.127\, m_b^2 \qquad m_b > 5.5$$

$$M_{w2} = 3.45 - 0.473*m_b + 0.145*m_b^2$$

$$M_{w3} = A + B - (p/3)$$
where
$$p = -22.21$$
$$a = 13.22$$
$$b = 206.0 - 29.10*m_b$$

$$A = \sqrt[3]{-\frac{b}{2}+\sqrt{\frac{b^2}{4}+\frac{a^3}{27}}}$$

$$B = \sqrt[3]{-\frac{b}{2}-\sqrt{\frac{b^2}{4}+\frac{a^3}{27}}}$$

If given M_w and need m_b, then

$$m_b = (m_{b1} + m_{b2} + m_{b3})/3$$

where

$$m_{b1} = 0.398 + 1.0204 * M_w \qquad\qquad M_w \leq 5.0$$
$$= 1.091 + \sqrt{7.874 * M_w - 20.19} \qquad M_w > 5.0$$

$$m_{b2} = 1.631 + \sqrt{6.897 * M_w - 21.133}$$

$$m_{b3} = -10.23 + 6.105 * M_w - 0.7632 * M_w^2 + 0.03436 * M_w^3$$

The M_{w1} relationship is from Atkinson and Boore (SSAR Reference 2.5.2-13). The M_{w2} relationship is from Frankel et al. (SSAR Reference 2.5.2-14). The m_{b3} is from EPRI (SSAR Reference 2.5.2-15). The corresponding mathematical inversions of these are the relations for m_{b1}, m_{b2}, and M_{w3}, respectively.

The M_{w2} relationship from Frankel et al. relationship starts to bend upward unrealistically for m_b less than 1.75, and probably should not be used for magnitudes less than m_b 3.0.

Due to the nonlinearity of the averaging of these relationships, converting an m_b to M_w and then using that M_w to convert back to m_b does not precisely return back the starting m_b value. The same M_w-m_b-M_w difference occurs. For m_b or M_w of 4 and greater, this effect is very small – about 1% or less. For m_b or M_w of 3.3 the difference is about 3 to 6%.

SSAR Table 2.5.2-1 provides a tabulation of selected paired magnitude values developed from these relationships, and may be used in lieu of the formulae.

Reference

1. Davis, S, P. Nyffenegger, and C. Frohlich (1995) "The 9 April 1993 Earthquake in South-Central Texas: Was It Induced by Fluid Withdrawal?". Bulletin of the Seismological Society of America, Vol. 85, No. 6, pp. 1888-1895.

Associated ESPA Revisions:

No ESPA revision is required as a result of this response.

RAI 02.05.02-2:

Question:

In SSAR Section 2.5.2.1, the applicant discussed its seismicity catalog completeness analysis. In accordance with 10 CFR 100.23, the staff requests the applicant provide additional information regarding its seismicity catalog.

SSAR Section 2.5.2.1.5 describes how the catalog completeness analysis was extended to the Gulf of Mexico region following the catalog update. A *b*-value of 1.05 is derived, but its region of applicability is not clearly stated. Please provide a map showing EPRI Incompleteness Region 2 and 3 and the region of the Gulf of Mexico where the updated completeness model applies. In addition, please describe in detail the method used to compute the *b*-value and clarify whether the *b*-value of 1.05 applies to the "project seismicity investigation window" region (SSAR Figure 2.5.2-1), only the "Gulf of Mexico seismicity recurrence area" (SSAR Figure 2.5.2-3), or some other regions.

Response:

Figure 1 shows the EPRI Incompleteness Regions, as slightly modified from Table 5.1 in SSAR Reference 2.5.2-18. The region of the Gulf of Mexico, where the updated periods of completeness model applies, is indicated in SSAR Figure 2.5.2-3 as the "Gulf of Mexico seismicity recurrence area".

The discussion below presents a summary of the maximum-likelihood method used to develop the b-value of 1.05 for the Gulf of Mexico seismicity recurrence area. It is important to note, however, that this calculation of b-value was performed as a confirmation of the development of the matrix of detection probabilities of SSAR Table 2.5.2-6. That is, this calculation was performed to confirm that using this matrix of detection probabilities with the seismicity observed in the Gulf of Mexico seismicity recurrence area, as tabulated in SSAR Table 2.5.2-4, results in a reasonable b-value. The resulting b-value of 1.05 is a reasonable b-value given that global b-values are observed to range from 0.8 to 1.2, as discussed in SSAR Section 2.5.2.1.5.

For the probabilistic seismic hazard analysis (PSHA), however, this b-value was not used. As discussed in SSAR Section 2.5.2.4.2.2, the EPRI EQPARAM software was used to calculate seismicity parameters (a- and b-values of Gutenberg-Richter relationship given the form log N = a − bM, where N is the number of earthquakes in a given period larger than magnitude M) for degree cells in the Gulf of Mexico seismicity recurrence area using the seismicity data (SSAR Table 2.5.2-4) and matrix of detection probabilities (SSAR Table 2.5.2-6) that were not available in the original EPRI-SOG database.

Confirmation Calculation of b = 1.05

The Gulf of Mexico seismicity of SSAR Table 2.5.2-4 is applied to the detection probability matrix of SSAR Table 2.5.2-6 in the manner presented in SSAR Reference 2.5.2-3 to develop completeness-corrected earthquake statistics. Basically, using the magnitude-year bins given in SSAR Table 2.5.2-6, seismicity counts of the events given in SSAR Table 2.5.2-4 are tabulated. For each magnitude bin the summation over the time period bins of the product of the detection probability and the number of years for each time bin gives the "effective completeness years" for that magnitude bin. Again for each magnitude bin, the sum of the number of events in time bins associated with non-zero probability of detection, divided by the effective completeness years for that magnitude bin gives the "bin annual rate" of events for that magnitude bin.

Given the completeness-corrected annual rates for each magnitude bin, the method of maximum-likelihood estimation of b-value, as first derived by Weichert (Reference 1) and then described by McGuire (Reference 2), was used. The maximum-likelihood estimate of the b-value is determined using the following equation presented in McGuire (Reference 2, Eq. A5, p. 190):

$$M_{bar} = \frac{\sum_i T_{E,i} M_{MID,i} e^{-\beta M_{MID,i}}}{\sum_i T_{E,i} e^{-\beta M_{MID,i}}}$$

where

i	is the index of the magnitude bin
$T_{E,i}$	is the effective period of completeness for magnitude bin i
$M_{MID,i}$	is the mid-range magnitude value of magnitude bin i
β	= b•ln(10)
M_{bar}	is the average magnitude of all of the events in magnitude bins associated with non-zero detection probabilities, using the $M_{MID,i}$ value of magnitude

In the equation above, "b" is solved recursively, resulting in a value of 1.05.

Table 5-1

EPRI PARAMETER FILE (abridged)

```
25.,52.,55.,107.,27,52,13      Incompleteness regions: boundaries, no. of intervals, etc.
14                             number of regions for symbols will be entered
0123456789ABCD                 symbols for incompleteness regions
0,1,2,3,4,5,6,7,8,9,10,11,12,13  numbers for incompleteness regions
000111000000000000000000BBB000000000000BBBBB000000
000112000000000B000000000BBB000BB00009999BBBBB000000
111122000000000020000000BBBB000BBB9999999BBBBB000000
111122000000000200000000BBBBB9999999AAA99999BBB000000
11112200000000222200000999999999AAAAA99999999000000
111122200002222222220000099999AAA555AAAAAAAAA99900000
111112200023333333330000999AAAAA555AAAAAAAAA99988888
11111122222333333333300004AAA5555555555AA99AA00000888
11111122222333333334340044AA5556566665AA9999900000000
111111222233333334444444444555555566666579998800000000
11122222233333334444444444555555666665798880000000000
222222222333333444444444445555556666557779880000000000
2222222222333334444444444CCCCC66557779888800000000000
2222222222333333444444444CCCCC65577798000000000000000
222222222333333334444444433CCC6677700000000000000000
2222222233333333334444433333CCCCC7700000000000000000
222222233333333333344433333CCC77000000000000000000
2212222233333333333333333333C770000000000000000000
111122222333333333333333333CC33D000000000000000000
1111122223333333333333333333D0000000000000000000
11111222333333333333333333D0D000000000000000000
0110000033323333333332221BDD0000000000000000000
0100000032222300000000000CDDD00000000000000000000
0000000022220000000000000CDDD000000000000000000
0000000000000000000000000CDDD00000000000000000000
000000000000000000000000CDDD000000000000000000000
0000000000000000000000000DDD00000000000000000000
3.3,7.5,7,0,0.0      Lowest mag., highest mag., no. of mag. intervals; KUNC=0
```

Map of incompleteness regions; covers region specified in line 1; uses symbols specified in line 3. Region 0 is not modeled

Figure 1 Modified portion of Table 5-1 of SSAR Reference 2.5.2-18 (EQHAZARD Primer).

Note: Highlighted (red) boundary indicates limit of southern extent of EPRI-SOG seismicity characterization. The matrix of numbers (Incompleteness Regions) is distributed in 1° longitude by 1° latitude values, where the lower left corner corresponds to (-107°E, 25°N). SSAR Reference 2.5.2-26 indicates that "grid locations for which the associated number is zero are not considered in the EQPARAM analysis". (The EPRI computer program EQPARAM develops earthquake recurrence parameters for the PSHA).

References

1. Weichert, D. H. (1980). Estimation of the earthquake recurrence parameters for unequal observation periods for different magnitudes. Bulletin of the Seismological Society of America, Vol. 70, No. 4, pp. 1337-1346.

2. McGuire, R. (2004). Seismic Hazard and Risk Analysis. Earthquake Engineering Research Institute, Monograph Series, MNO-10, 221p.

Associated ESPA Revision:

No ESPA revision is required as a result of this response.

RAI 02.05.02-7:

Question:

In SSAR Section 2.5.2.4, the applicant discussed the probabilistic seismic hazard analysis (PSHA) conducted for the VCS site. In accordance with 10 CFR 100.23, the staff requests the applicant provide additional information regarding its PSHA.

SSAR Section 2.5.2.4.7 describes how the applicant developed its low-frequency (LF) and high-frequency (HF) Uniform Hazard Spectral (UHS) shapes. Please explain the methodology used by the applicant to develop the smooth UHS. In addition, explain why the LF spectrum might exceed the HF spectrum at high frequencies and why this was not allowed.

Response:

The smooth hard rock 10^{-4}, 10^{-5}, and 10^{-6} annual frequencies of exceedance uniform hazard response spectra (UHRS) of the SSAR were developed from the 100 Hz, 25 Hz, 10 Hz, 5 Hz, 2.5 Hz, 1 Hz, and 0.5 Hz spectral acceleration values taken from the probabilistic seismic hazard analysis (PSHA) curves. To generate smooth spectral values between the directly calculated PSHA values at these seven frequencies LF and HF spectral shapes were computed based on the mean deaggregation magnitude and distance values listed in Table 2.5.2-25 of the SSAR and the median hard rock central and eastern United States (CEUS) spectral shapes given in NUREG/CR-6728 (SSAR Reference 2.5.2-2). As described in SSAR Section 2.5.2.4.7, the HF spectral shape was anchored to the UHRS values at frequencies of 100 Hz, 25 Hz, 10 Hz, and 5 Hz. Similarly, the LF spectral shape was anchored at all seven of the ground-motion frequencies for which the seismic hazard calculations were performed to prevent the LF spectra when extrapolated to high frequencies to exceed the directly computed PSHA values.

UHRS values for frequencies between these seven frequencies were taken as the envelope of these HF and LF spectra interpolated between the seven computed PSHA values based on an inverse logarithmic difference between bounding frequencies and ground-motion values. These smoothed UHRS spectra values are listed in Table 1.

Table 1. Smooth UHRS based on the envelope of the HF and LF spectral
shapes described above

Frequency (Hz)	10^{-4} Smoothed UHS	10^{-5} Smoothed UHS	10^{-6} Smoothed UHS
100.	3.10E-02	1.32E-01	5.57E-01
90.	3.38E-02	1.46E-01	6.16E-01
80.	3.87E-02	1.69E-01	7.15E-01
70.	4.62E-02	2.04E-01	8.67E-01
60.	5.57E-02	2.50E-01	1.06E+00
50.	6.48E-02	2.96E-01	1.26E+00
45.	6.85E-02	3.16E-01	1.35E+00
40.	7.13E-02	3.32E-01	1.42E+00
35.	7.32E-02	3.44E-01	1.47E+00
30.	7.42E-02	3.53E-01	1.51E+00
25.	7.43E-02	3.56E-01	1.52E+00
20.	7.38E-02	3.43E-01	1.42E+00
15.	7.12E-02	3.15E-01	1.25E+00
12.5	6.85E-02	2.92E-01	1.12E+00
10.	6.44E-02	2.60E-01	9.58E-01
9.	6.40E-02	2.52E-01	9.05E-01
8.	6.33E-02	2.43E-01	8.46E-01
7.	6.21E-02	2.31E-01	7.80E-01
6.	6.03E-02	2.16E-01	7.04E-01
5.	5.77E-02	1.99E-01	6.15E-01
4.	5.51E-02	1.86E-01	5.32E-01
3.	5.22E-02	1.64E-01	4.25E-01
2.5	5.08E-02	1.48E-01	3.57E-01
2.	4.73E-02	1.40E-01	3.24E-01
1.5	4.31E-02	1.29E-01	2.85E-01
1.25	3.99E-02	1.20E-01	2.58E-01
1.	3.75E-02	1.07E-01	2.26E-01
0.9	3.68E-02	1.11E-01	2.32E-01
0.8	3.56E-02	1.12E-01	2.36E-01
0.7	3.37E-02	1.10E-01	2.36E-01
0.6	3.24E-02	1.09E-01	2.37E-01
0.5	3.05E-02	1.06E-01	2.31E-01
0.4	2.21E-02	7.71E-02	1.68E-01
0.3	1.40E-02	4.91E-02	1.08E-01
0.2	6.60E-03	2.32E-02	5.12E-02
0.15	3.50E-03	1.23E-02	2.72E-02
0.125	2.22E-03	7.82E-03	1.72E-02
0.1	1.19E-03	4.18E-03	9.17E-03

Figures 2.5.2-42 through 2.5.2-47 of the SSAR graphically show the deaggregation results from the PSHA for the three annual frequencies of exceedance (i.e., 10^{-4}, 10^{-5}, and 10^{-6}) for the mean ground motions at 1 Hz and 2.5 Hz (LF), and 5 and 10 Hz (HF) cases. In these deaggregation plots the contribution to hazard from different ε bins (i.e., number of standard deviations that the value is above the mean) is color coded, and the general conclusion is noted that the total 10^{-4} and 10^{-5} ground motions have significant 0 to 2 ε contributions. In addition, the LF results indicate a larger percentage of total ground motion hazard from higher relative ε bins when compared to the HF results.

As described in the SSAR Section 2.5.2.4.7, LF and HF spectral shapes were computed based on the mean deaggregation magnitude and distance values listed in Table 2.5.2-25 of the SSAR and the median hard rock central and eastern United States (CEUS) spectral shapes given in NUREG/CR-6728 (SSAR Reference 2.5.2-2). Given that the

CEUS hard rock spectral shapes in NUREG/CR-6728 are median spectral shapes, the development of HF and LF spectral shapes would not be expected to be consistent in cases in which the ε contribution is different between the two HF and LF cases. Stated another way, if the contribution for the HF and LF to the hazard was predominately from ε approximately equal to zero (i.e., median values), the median spectral shapes based on these controlling magnitude and distance values should be approximately equal to the hazard ground motions over all of the frequencies.

For the development of the mean HF spectral shapes, the controlling magnitude and distance values (SSAR Table 2.5.2-25) were used with the CEUS hard rock spectral shape model from NUREG/CR-6728 (SSAR Reference 2.5.2-2). The additional constraint was applied where the scaled spectral shape was anchored to the high frequency ground-motion values at frequencies of 100 Hz, 25 Hz, 10 Hz, and 5 Hz. For lower frequencies (i.e., less than 5 Hz), the resulting scaled median spectral shape was less than the ground-motion values computed from the hazard. This is shown in Figures 2.5.2-48 and 2.5.2-49 of the SSAR for the 10^{-4} and 10^{-5} annual frequencies of exceedance, and is the result of the relative lower spectral shape for low frequencies (i.e., less than 5 Hz) and intermediate to smaller magnitudes estimated from the NUREG/CR-6728 model than the controlling events from the hazard.

For the development of the mean LF spectral shapes, the same approach with the anchoring of the LF spectral shapes to the low frequency ground-motion values (i.e., 2.5 Hz, 1 H and 0.5 Hz) would lead to associated high frequency ground motions, which would exceed the ground motions from the direct PSHA hazard. This is a consequence of low frequency motions from the hazard being controlled by results with relatively larger ε values than the high frequency results. Given the relatively larger ε values and the scaling of the median spectral shape anchored to these low frequency ground-motion values, the resulting high frequency motions exceed the hazard at high frequency motions.

The results are shown in Figure 1 for the 10^{-4} mean HF and LF spectral case. The LF spectrum in this figure clearly predicts higher ground motions for the high frequency range between 5 Hz and 100 Hz when the spectrum is only anchored to the low frequency ground-motion values. However, based on the HF and LF rock spectra being used as input ground-motion spectra for the development of site amplification factors (SAF), the LF spectrum was anchored to all of the seven ground-motion frequencies used in the hazard.
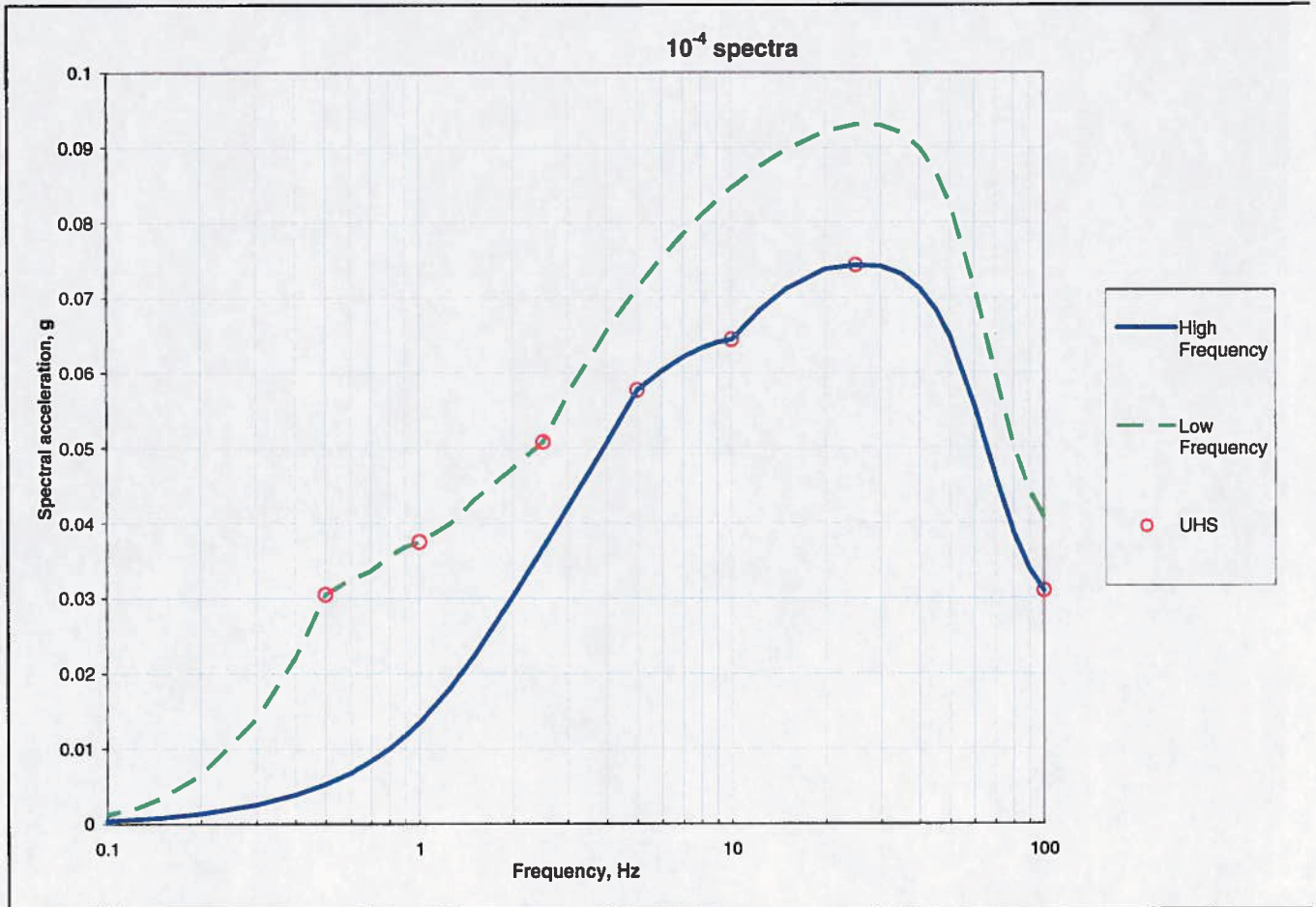
Figure 1. Comparison of HF and LF rock spectra for 10^{-4} where the LF spectrum is only anchored to the low frequency ground-motion values. Note that this LF spectrum was not recommended and used in the site response analysis.

Finally, it should be noted that uncritical acceptance of extrapolated LF spectral shape to high frequencies, and the consequent increase of the high frequency part of the spectra beyond UHRS values developed from the PSHA analysis could overdrive the soil column during the site response analysis, which could lead to lower site amplification factors.

Associated ESPA Revision:

No ESPA revision is required as a result of this RAI response.

RAI 02.05.02-8:

Question:

In SSAR Section 2.5.2.4, the applicant discussed the probabilistic seismic hazard analysis (PSHA) conducted for the VCS site. In accordance with 10 CFR 100.23, the staff requests the applicant provide additional information regarding its PSHA.

Please discuss and justify which EPRI 2004 ground motion model (Mid-Continental, Gulf Coastal, or others) the applicant used to characterize the VCS rock hazard for each seismic source – the individual EPRI sources, the NMSZ, the Meers fault, and the RGR.

Response:

For the EPRI team sources, the Gulf equations from the EPRI 2004 model were used, because the VCS site lies well within the Gulf region as depicted in Figure 3-2 of EPRI 2004, and earthquakes within about 20 to 60 km of the site dominate the contribution to hazard from local earthquakes (see, for example, SSAR Figures 2.5.2-42 through 2.5.2-47, which show the contribution to hazard by magnitude and distance). For the New Madrid seismic zone (NMSZ), the Mid-continent equations from the EPRI 2004 model were used. This choice is conservative, because although the NMSZ lies within the Mid-continent region (see Figure 3-2 of EPRI 2004), most of the travel path of seismic waves will be through the Gulf region for earthquakes occurring on this source. For the Meers fault, the Gulf equations from the EPRI 2004 model were used, because the site lies within the Gulf region. Some argument could be made that the Mid-continent equations should be used for the Meers fault, because of the travel path of seismic waves from potential earthquakes on this source. However, SSAR Figures 2.5.2-18 and 2.5.2-19 (calculated using the Gulf equations) show that the Meers fault hazard is more than 4 orders of magnitude below the total hazard calculated for the VCS (at amplitudes where the total hazard is 1×10^{-4} and less). It is not likely that using Mid-continent equations would change the conclusion that the Meers fault contributes an insignificant hazard to the VCS site. For the Rio Grande Rift faults, the Gulf equations from the EPRI 2004 model were used, because the site lies within the Gulf region and the predominant travel path of seismic waves is through the Gulf region, particularly for faults representing the southern extension of the Rio Grande Rift faults that lie closest to the site.

References:

EPRI (2004). *CEUS Ground Motion Project Final Report,* Electric Power Research Institute, Report. 1009684, Palo Alto, CA, December 2004.

Associated ESPA Revision:

No ESPA revision is required as a result of this RAI response.

RAI 11.02-3:

Question:

10 CFR 20, 10 CFR 50 Appendix I, SRP 11.2, and RG 1.109 require that certain parameters to calculate the liquid effluent off-site dose to the public be identified for review and evaluation on a per unit basis.

In Table 11.2.3-1 (Sheet 1 of 3), the Discharge Flow Rate value is listed as 480 cubic feet per second (cfs), but does not specify in the basis whether this flow rate is used for one unit, two units, or the site.

Please verify and note in the application whether the value listed for the Discharge Flow Rate in Table 11.2.3-1 is for one unit, two units or the site. Please explain the following parameters within the application, 1) the river flow rate and 2) the liquid effluent release rate. Please verify and note in the application table that a discharge flow rate value on a per unit basis will be used in this application since the release source term and effluent doses are calculated on a per unit basis.

Response:

The Discharge Flow Rate value of 480 cfs in SSAR Table 11.2.3-1 is actually the Guadalupe River flow rate. Hence, it is independent of the number of units releasing effluents. Since the effluent flow characteristics in the ESP application are for a bounding scenario rather than a specific reactor design, it is conservatively assumed that the effluent activity is diluted by river flow only. Table 11.2.3-1 (Sheet 1 of 3) is revised to clarify that 480 cfs is the Guadalupe River flow rate.

In response to RAI 11.02-1, Table 11.2.3-3 is revised to clarify that releases in the table are per unit but the calculated river concentrations are for all units on site. Please note that each dose table currently specifies whether it is on a per unit basis or for all units on site.

Associated ESPA Revision:

The changes to SSAR Table 11.2.3-1 are shown on the following page.

Corresponding ER Table 5.4-1 is also being revised with identical language to clarify that 480 cfs is the flow rate for the Guadalupe River. Note that the ER Table 5.4-1 entry to be revised is labeled "Flow Rate in Receiving Water Body," versus the label of "Discharge Flow Rate" used in SSAR Table 11.2.3-1. The ER revisions will be made in the next update of the ESPA.

Table 11.2.3-1 (Sheet 1 of 3)
Liquid Pathway Parameters

Parameter	Value	Basis/Source(s)
Release Source Terms	See Table 11.2.3-2	Table 11.2.3-2 shows the activity releases by isotope.
Impoundment Reconcentration Model	None	This model does not apply to the river discharge scenario.
Individual Consumption/ Exposure Rates	See RG 1.109	The values from Tables E-5 and E-4 of RG 1.109 are used for the MEI and the average person within the population, respectively.
Site Water Type	River	Guadalupe River.
Discharge Flow Rate	480 cfs	This is a conservative flow rate that represents the 95th percentile of all observed annual average flow rates in the Guadalupe River from 1935 to 2008. Effluent activity is assumed to be released directly into the river without any prior dilution.
Shore-Width Factor	0.2	This is the appropriate value for a river (RG 1.109, Table A-2).
Dilution factor for Discharge	1	No dilution is assumed beyond mixing in the river flow rate.
Transit Time to Receptor	See RG 1.109	The default transit times from RG 1.109, Table D-1 are used.
Irrigation Rate	110 l/m^2 per month	Based on an assumed value of 1 inch per week.
50-Mile Population	4.15×10^5	This is the projected population for the year 2080, the assumed end of plant life. It is used to conservatively maximize population doses. This projection represents an increase of a factor of 1.7 over the 2000 population.
50-Mile Drinking Water Population	7.08×10^4	Of the municipal water usage in the 12 counties within 50 miles of the plant, 17% comes from the Guadalupe River (Reference 11.2.3-2). Based on this, it is assumed that 17% of the population in 2080 receives its drinking water from Guadalupe River.
50-Mile Sport Fishing Harvest	6.69×10^4 kg/yr	Based on RG 1.109, Appendix D and Table E-4, the average individual consumes 5.9 kg/yr of fish. Multiplying this by the 2080 population yields the total annual consumption of fish within 50 miles of 2.43 $\times 10^6$ kg/yr. Of the state population of 20.9 million (Reference 11.2.3-3), 0.574 million (Reference 11.2.3-4) or about 2.75% engages in sport fishing in rivers. It is assumed that 2.75% of the fish consumption within 50 miles is due to sport fishing from Guadalupe River.
50-Mile Commercial Fishing Harvest	1.15×10^6 kg/yr	As the previous entry indicates, of the total fish consumption within 50 miles of 2.43 $\times 10^6$ kg/yr, 2.75% is due to sport fishing. It is assumed that Guadalupe River is the source of 50% of the fish consumed within 50 miles, with the remaining 47.25% coming from commercial fishing.
50-Mile Sport Invertebrate Harvest	9.71×10^3 kg/yr	Based on RG 1.109, Appendix D and Table E-4, the average individual consumes 0.85 kg/yr of invertebrate. Multiplying this by the 2080 population yields the total annual consumption of invertebrate within 50 miles of 3.53 $\times 10^5$ kg/yr. As with sport fishing, it is assumed that 2.75% of the invertebrate consumption within 50 miles is due to sport invertebrate harvest from the Guadalupe River.
50-Mile Commercial Invertebrate Harvest	1.67×10^5 kg/yr	As the previous entry indicates, of the total invertebrate consumption within 50 miles of 3.53 $\times 10^5$ kg/yr, 2.75% is due to sport invertebrate harvest. It is assumed that Guadalupe River is the source of 50% of the invertebrate consumed within 50 miles, with the remaining 47.25% coming from commercial harvest.

RAI 11.02-4:

Question:

40 CFR 190 requires that the individual dose equivalent to any member of the public from all nuclear fuel cycle facilities be considered against the limits of 40 CFR 190 and 10 CFR 20.1301(e). Table 11.2.3-6 in the VCS ESP application lists the total dose to any member of the public from all facilities, but does not give a breakdown of each facility and its contribution to each total dose.

Please include a breakdown of all doses: total body, thyroid and any other organ, to any member of the public as the result of exposures to planned discharges of radioactive material for each nuclear fuel facility included within the ESP application. Also, compare the total of these breakdowns to the 40 CFR 190 limits.

Response:

SSAR Table 11.2.3-6 for Liquid Releases, as well as Table 11.3.3-7 for Gaseous Releases, shows total site doses based on two units. The individual unit doses are calculated based on a conservative, bounding composite source term of the various reactor technologies as discussed in Sections 11.2.3.2 and 11.3.3.2. These composite source terms are shown in Tables 11.2.3-2 and 11.3.3-2.

A footnote is added to Table 11.2.3-6 as well as corresponding Table 11.3.3-7 to explain how the values within the table are obtained.

While preparing the footnote, an error was discovered in one of the table values. The site doses due to gaseous effluents from two units are supposed to be obtained by doubling the larger of the site boundary and maximally exposed individual (MEI) doses that are presented in Table 11.3.3-5 for a single unit. While the total body and bone doses are correctly calculated, the thyroid dose was shown as double of the site boundary dose of 7.8 mrem rather than double of the larger MEI dose of 13 mrem. Tables 11.2.3-6 and 11.3.3-7 are revised to show a correct site thyroid dose of 25 mrem.

When the revised gaseous effluent dose is added to the liquid effluent and direct radiation doses, the site thyroid dose becomes 32 mrem, which is within the 40 CFR 190 limit of 75 mrem.

Associated ESPA Revision:

The changes to SSAR Tables 11.2.3-6 and 11.3.3-7 are shown on the following pages.

Also, the following reference is added to Subsection 11.2.3.3:

11.2.3-8   *ABWR Design Control Document*, Tier 1, GE Nuclear Energy, Revision 4, 1997.

The following reference is added to Subsection 11.3.3.3:

> 11.3.3-4   *ABWR Design Control Document*, Tier 1, GE Nuclear Energy, Revision 4, 1997.

Corresponding ER Table 5.4-7 is also being revised to correct the thyroid dose. Additionally, the following explanatory footnote will be added to ER Table 5.4.7 as note "(b)":

> Site doses for two units are obtained by doubling the doses from a single unit. Liquid effluent doses are obtained by doubling the doses in Table 5.4-4. Gaseous effluent doses are obtained by doubling the higher of site boundary and MEI doses in Table 5.4-5. The direct radiation dose is obtained by doubling 2.5 mrem/yr, the dose outside the controlled area corresponding to the shielding criteria for the ABWR (GE 1997, Table 3.2a); this is the largest direct dose component for the reactor technologies being evaluated.

The ER revisions will be made in the next update of the ESPA.

Table 11.2.3-6
Comparison of Maximally Exposed Individual Doses
with 40 CFR 190 Criteria

	Site Dose for All Units (mrem/yr)				
	Liquid	Gaseous	Direct	Total	Limit
Total Body	1.5	5.8	5.0	12	25
Thyroid	1.3	~~16~~25	5.0	~~22~~32	75
Other Organ — Bone	2.6	11	5.0	19	25

Note: Site doses for two units are obtained by doubling the doses from a single unit. Liquid effluent doses are obtained by doubling the doses in Table 11.2.3-4. Gaseous effluent doses are obtained by doubling the higher of site boundary and MEI doses in Table 11.3.3-5. The direct radiation dose is obtained by doubling 2.5 mrem/yr, the dose outside the controlled area corresponding to the shielding criteria for the ABWR (Reference 11.2.3-8, Table 3.2a); this is the largest direct dose component for the reactor technologies being evaluated.

Table 11.3.3-7
Comparison of Maximally Exposed Individual Doses
with 40 CFR 190 Criteria

	Site Dose for All Units (mrem/yr)				
	Liquid	Gaseous	Direct	Total	Limit
Total Body	1.5	5.8	5.0	12	25
Thyroid	1.3	~~16~~25	5.0	~~22~~32	75
Other Organ — Bone	2.6	11	5.0	19	25

Note: Site doses for two units are obtained by doubling the doses from a single unit. Liquid effluent doses are obtained by doubling the doses in Table 11.2.3-4. Gaseous effluent doses are obtained by doubling the higher of site boundary and MEI doses in Table 11.3.3-5. The direct radiation dose is obtained by doubling 2.5 mrem/yr, the dose outside the controlled area corresponding to the shielding criteria for the ABWR (Reference 11.3.3-4, Table 3.2a); this is the largest direct dose component for the reactor technologies being evaluated.

ATTACHMENT 8

SUMMARY OF REGULATORY COMMITMENTS

(Exelon Letter to USNRC, NP-11-0016, dated May 5, 2011)

The following table identifies commitments made in this document. (Any other actions discussed in the submittal represent intended or planned actions. They are described to the NRC for the NRC's information and are not regulatory commitments.)

COMMITMENT	COMMITTED DATE	COMMITMENT TYPE	
		ONE-TIME ACTION (Yes/No)	Programmatic (Yes/No)
Exelon will revise the VCS ESPA SSAR Section 2.4.6 to incorporate the change shown in the enclosed response to the following NRC RAI: 02.04.06-1 (Attachment 1)	Revision 1 of the ESPA SSAR and ER planned for no later than March 31, 2012	Yes	No
Exelon will revise the VCS ESPA SSAR Sections 11.2 and 11.3, and ER Section 5.4, to incorporate the changes shown in the enclosed responses to the following NRC RAIs: 11.02-3, 4 (Attachments 6 & 7)	Revision 1 of the ESPA SSAR and ER planned for no later than March 31, 2012	Yes	No